Halo-free quantitative phase imaging with partially coherent light

Tan H. Nguyen[a,b], Hassaan Majeed[a], Christopher A. Edwards[a,c], Minh N. Do[b],
Lynford L. Goddard[c], Gabriel Popescu*[a]

[a]Quantitative Phase Imaging Laboratory, Beckman Institute for Advanced Science and Technology, Dept. of Electrical and Computer Engineering, Univ. of Illinois at Urbana-Champaign, IL USA 61801.
[b]Computational Imaging group, Coordinated Science Laboratory, Dept. of Electrical and Computer Engineering, Univ. of Illinois at Urbana-Champaign, IL USA 61801.
[c]Photonic Systems Laboratory, Micro and Nanotechnology Laboratory, Dept. of Electrical and Computer Engineering, Univ. of Illinois at Urbana-Champaign, IL USA 61801.

ABSTRACT

We provide a quantitative model for image formation in common-path QPI systems under partially coherent illumination. Our model is capable of explaining the phase reduction phenomenon and halo effect in phase measurements. We further show how to fix these phenomena with a novel iterative post-processing algorithm. Halo-free and correct phase images of nanopillars and live cells are used to demonstrate the validity of our method.

Keywords: Phase Imaging, holography, image processing, halo removal, computational imaging

1. INTRODUCTION

Common-path interferometric QPI modalities e.g. Diffraction Phase Microscopy (DPM) [1, 2], Fourier Phase Microscopy (FPM) [3] and Spatial Light Interference Microscopy (SLIM) [4, 5] have become increasingly popular alongside with *traditional* interferometric ones [6-10], thanks to their high stability (spatial and temporal) [11]. The most important benefit of these methods compared to traditional QPI is the ability to be deployed onto existing commercial microscopes as add-on modules. In common-path QPI, the reference field $\mathbf{U}_r$ is generated by spatially low-pass filtering the total field, $\mathbf{U}_t$, i.e. $\mathbf{U}_r = \mathbf{U}_t \oslash h_o$ with some low-pass filter h_o. The total field, $\mathbf{U}_t$, is a modulated version of the incident field, $\mathbf{U}_i$, with the modulation function given by the object transmission $T(\mathbf{r})$ namely $\mathbf{U}_t(\mathbf{r}) = \mathbf{U}_i(\mathbf{r})T(\mathbf{r})$. Common-path QPI methods quantify the temporal cross-correlation between the reference field and the total field for each coordinate $\mathbf{r}$ at zero temporal delay $\tau = 0$. Therefore, the measured quantity in common-path QPI is given by

$$\Gamma_{r,t}(\mathbf{r},\mathbf{r},0) = \left\langle \mathbf{U}_t(\mathbf{r},t)\mathbf{U}_r^*(\mathbf{r},t) \right\rangle, \tag{1}$$

where the angular bracket denotes ensemble average. Figure 1 shows an example of the DPM setup. First, the total field is relayed to the output port of a commercial microscope. A diffraction grating is used to generate two different orders of the total fields. The zero-order is spatially filtered by a physical pinhole placed at the back focal plane of a Fourier lens (here, lens L_2) to generate the reference field U_r. This reference field interferes with the second replica of the total field, which comes from the first diffraction order of the grating.
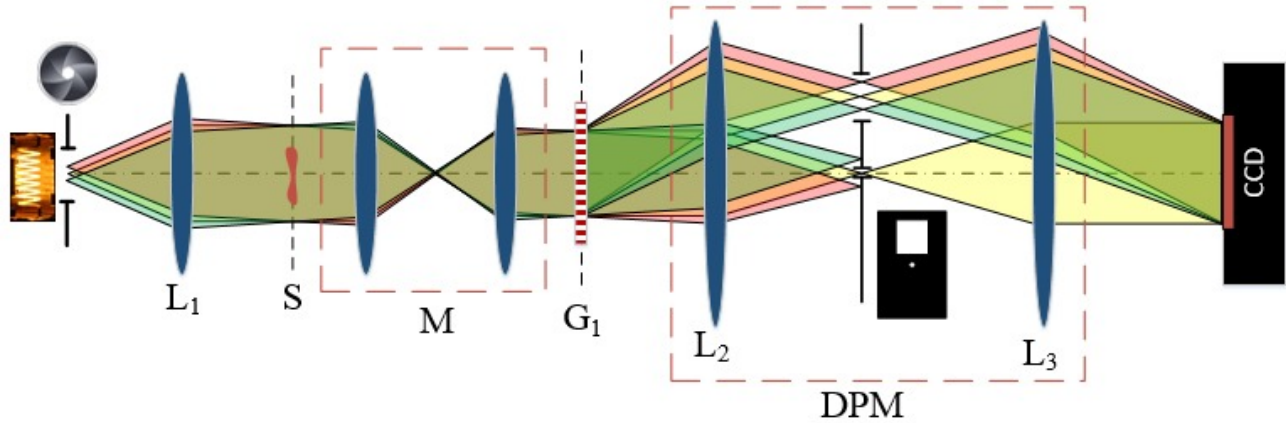
Figure 1. Diffraction phase microscopy setup

The temporal cross-correlation $\Gamma_{t,r}$ can be related to the transmission T as [12]

$$\Gamma_{r,t}(\mathbf{r},\mathbf{r},0) = T\left[T\circledcirc h_i\right]^*(\mathbf{r}),\tag{2}$$

where h_i is the product between the reference generating filter h_o and the spatial correlation function of the illumination Γ_i i.e. $h_i = h_o\Gamma_i$. From Eq. (2), the measured quantity in QPI, $\phi_m(\mathbf{r}) = \arg\left[\Gamma_{t,r}(\mathbf{r},\mathbf{r},0)\right]$, relates to the "true" phase quantity of interest, $\phi(\mathbf{r}) = \arg\left[T(\mathbf{r})\right]$, as

$$\phi_m(\mathbf{r}) = \phi(\mathbf{r}) - \arg\left[\left(T\circledcirc h_i\right)(\mathbf{r})\right].\tag{3}$$

Therefore, the measured phase value ϕ_m underestimates the true phase value ϕ by a low-pass version of the true phase $\arg\left[\left(T\circledcirc h_i\right)(\mathbf{r})\right]$ [13]. Note that when the illumination is fully coherent and the filtering is perfect i.e. $h_i \approx$ const., the underestimated amount is simply a constant and phase underestimation can be corrected by a simple background subtraction step. For incoherent illumination, $h_i \approx \delta$ and $\arg\left[\left(T\circledcirc h_i\right)(\mathbf{r})\right] \approx \arg\left[T(\mathbf{r})\right]$ which tells that $\phi_m \approx 0$, i.e. a phase measurement is impossible with fully incoherent illumination. Phase measurement for intermediate cases between these two extremes suffer from phase underestimation and the halo effect, which is well-known in phase contrast microscopy [13, 14]. In the next Section, we demonstrate how to fix for this underestimation and recover correct phase values.

2. NUMERICAL METHOD FOR HALO REMOVAL

2.1 Recovery of sample transmission function

Given correlation measurements $\Gamma_{r,t}$ and the filter h_i, the recovery problem of the sample transmission T using Eq. (2) is not obvious since the relation is nonlinear. Here, we suggest solving for T indirectly through the following joint optimization problem

$$\begin{aligned}\left\{T^\dagger, G^\dagger\right\} &= \arg\min_{T,G} f(T,G)\\ &= \arg\min_{T,G}\left\{\left\|\Gamma_{r,t} - TG^*\right\|_2^2 + \beta\left\|G - T\circledcirc h_i\right\|_2^2\right\},\end{aligned}\tag{4}$$

where β is the trade-off constant. The key point of solving Eq. (4) is the introduction of a new variable G to remove the nonlinearity of Eq. (2). Furthermore, the objective function, $f(T,G)$, is non-negative, quadratic and convex if we solve for a single variable T or G while fixing the other. Therefore, the following iterative alternating minimization algorithm ensures convergence to a local minimizer

Algorithm

- Initialize $T^{(0)}$ and the iteration index to $k = 0$.
- For $k \geq 1$, solve two sub-optimization problems and iterate until convergence

$$G^{(k)} = \arg\min_{G} f\left(T^{(k-1)}, G\right)$$

$$T^{(k)} = \arg\min_{T} f\left(T, G^{(k)}\right)$$

(5)

- At convergence at iteration k_o, return $T^{\dagger} = T^{(k_o)}, G^{\dagger} = G^{(k_o)}$.

2.2 Initialization and computational complexity

Note that the time complexity is proportional to the number of iterations. To minimize the computational cost, we start the first estimation $T^{(0)}$ to a good value. Here, we choose $T^{(0)}(\mathbf{r}) = \exp\left[i\phi^{(0)}(\mathbf{r})\right]$ where $\phi^{(0)}(\mathbf{r})$ is obtained by performing deconvolution on a linear approximation of Eq. (3): $\phi_m(\mathbf{r}) \approx \left[\phi^{(0)} \circledcirc \left(\delta^{(2)} - h_i\right)\right](\mathbf{r})$. Experimentally, the algorithm converges from 5-10 iterations with about 20 ms per iteration for images of size 2048x2048.

3. RESULTS

To demonstrate the efficiency of the proposed algorithm, we perform correction on a phase image of fabricated nanopillars. The sample is prepared from a 1'' quartz wafer patterned using SPR 511a positive photoresist and transferred to the quartz substrate by etching in a reactive-ion etcher (RIE) using a CF4 (Freon 14 plasma), resulting in square pillars of 20 micron wide and 80 nm high [13]. This height is verified by the Alpha Step IQ Profilometer. Figure 2 (a-b) shows original and corrected phase maps of the 80 nm thick nanopillars. It can be seen that before correction, most of the phase values in the center of the pillars are zeroed out and negative phase values appear surrounding the pillars. After correction, correct thickness values are obtained across the surface of the pillars. Erroneous negative phase values in the original halo regions are suppressed.
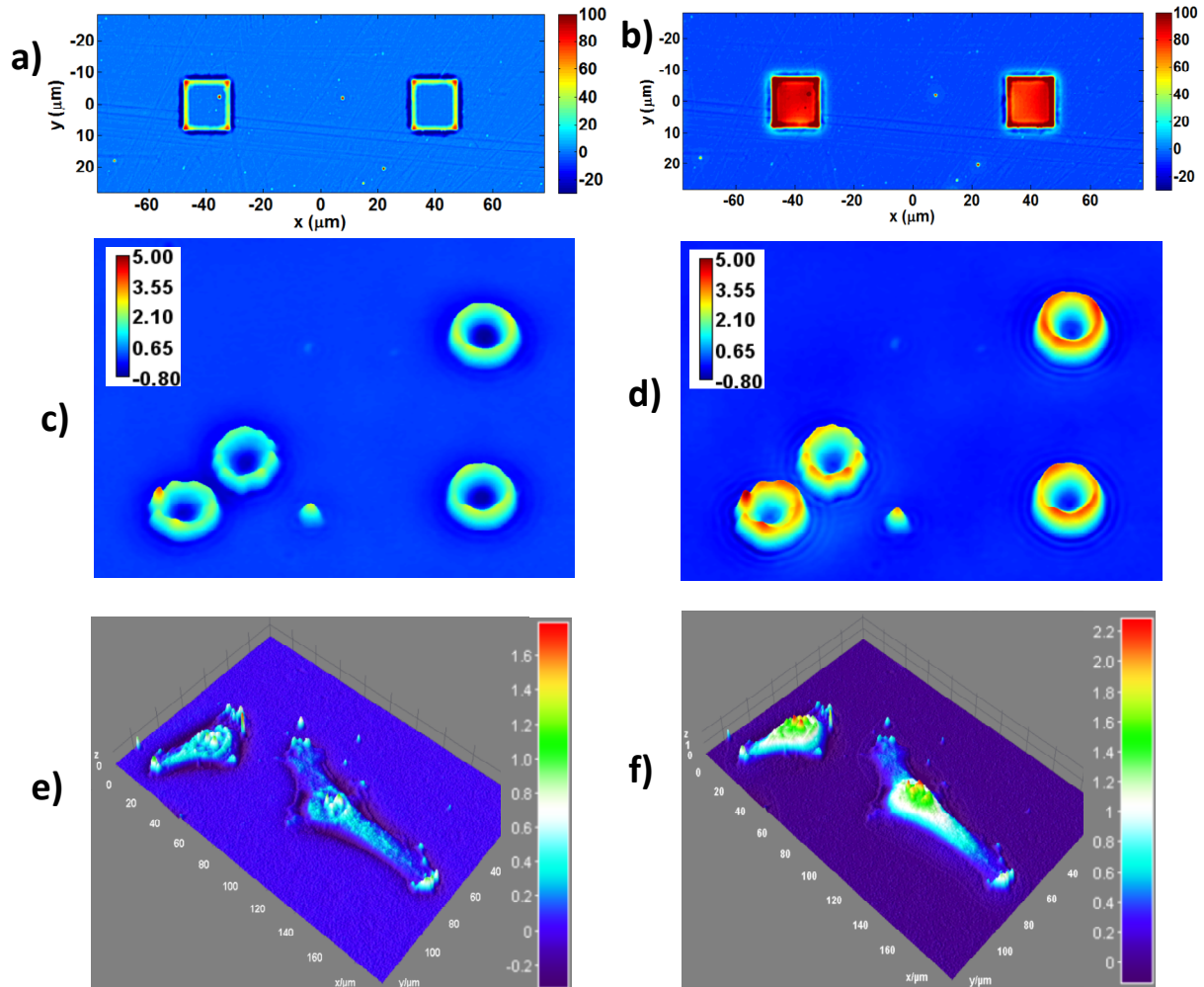
Figure 2. Original image and reconstruction phase maps of nanopillars (a - b), red blood cells (c-d) and HeLa cells (e-f).

Similarly, Fig. 2(c-d) show the original and reconstructed phase maps of the red blood cells. These cells were drawn from patients at our local hospital using venipuncture and stored in a refrigerator at 40°C prior to use. Before imaging, the whole blood sample was diluted to a concentration of 0.2% in PBSA solution (0.5% Bovine Serum Albumin (BSA) in PBS). A sample chamber was prepared by punching a hole into a piece of double sided scotch tape and sticking the tape onto a coverslip. After dispensing a drop of blood into this circular chamber, the drop was sealed from the top by a coverslip. The coverslip pair was then turned over and the cells were allowed to settle for 1 hr before measurement. It can be seen that reconstructed phase map has no halo and underestimated phase values are corrected. Finally, Figure 2 (e-f) are original and processed surface plots for the phase maps of the HeLa cells at about 30% confluence in a glass-bottom dishes (MatTek) with EMEM with 10% FBS. Again, negative phase values in the halo regions and underestimated phase values in the central areas of the cells are corrected.

4. SUMMARY AND FUTURE WORK

In this paper, we proposed a novel computational method to compensate for phase underestimations in partially coherent common-path QPI. Our method is based on an iterative algorithm to solve an optimization problem that minimizes the error between the measurements and the forward model. Our approach is verified on well-controlled fabricated samples. We also demonstrated success on fixing phase underestimation of live cells. Future efforts will be spent on optimizing the processing speed and making the algorithm more robust to optical aberrations and noise.

5. ACKNOWLEDGMENTS.

REFERENCES

[1] B. Bhaduri, C. Edwards, H. Pham *et al.*, "Diffraction phase microscopy: principles and applications in materials and life sciences," Advances in Optics and Photonics*,* 6(1), 57-119 (2014).

[2] B. Bhaduri, H. Pham, M.Mir *et al.*, "Diffraction phase microscopy with white light," Opt. Lett.*,* 37(11), (2012).

[3] G. Popescu, L. P. Deflores, J. C. Vaughan *et al.*, "Fourier phase microscopy for investigation of biological structures and dynamics," Optics Letters*,* 29(21), 2503-2505 (2004).

[4] Z. Wang, L. J. Millet, M. Mir *et al.*, "Spatial light interference microscopy (SLIM)," Opt. Exp.*,* 19(1016), (2011).

[5] T. H. Nguyen, and G. Popescu, "Spatial Light Interference Microscopy (SLIM) using twisted-nematic liquid-crystal modulation," Biomedical optics express*,* 4(9), 1571-1583 (2013).

[6] T. Ikeda, G. Popescu, R. R. Dasari *et al.*, "Hilbert phase microscopy for investigating fast dynamics in transparent systems," Opt. Lett.*,* 30(10), 1165-1167 (2005).

[7] D. Hogenboom, C. A. DiMarzio, T. J. Gaudette *et al.*, "Three-dimensional images generated by quadrature interferometry," Optics Letters*,* 23(10), 783-785 (1998).

[8] D. Zicha, and G. Dunn, "An image processing system for cell behaviour studies in subconfluent cultures," Journal of Microscopy*,* 179(1), 11-21 (1995).

[9] M. Somekh, C. See, and J. Goh, "Wide field amplitude and phase confocal microscope with speckle illumination," Optics communications*,* 174(1), 75-80 (2000).

[10] E. Cuche, F. Bevilacqua, and C. Depeursinge, "Digital holography for quantitative phase-contrast imaging," Opt. Lett.*,* 24(5), 291-293 (1999).

[11] G. Popescu, [Quantitative Phase Imaging of Cells and Tissues] Mcgraw-Hill, (2011).

[12] T. H. Nguyen, C. Edwards, L. L. Goddard *et al.*, "Quantitative phase imaging with partially coherent illumination," Optics Letters*,* 39(19), 5511-5514 (2014).

[13] C. Edwards, B. Bhaduri, T. Nguyen *et al.*, "Effects of spatial coherence in diffraction phase microscopy," Optics express*,* 22(5), 5133-5146 (2014).

[14] F. Zernike, "How I discovered phase contrast," Science*,* 121(3141), 345-349 (1955).